



Distorted Lattice Structure of La and Nd Co-Doped Bismuth Titanate $\text{Bi}_{3-x}\text{Ti}_4\text{O}_{12}$ Nano Grained Ceramics for High Quality Energy Storage Application

Md. Aminul Islam¹✉¹Department of Materials Science and Engineering, Rajshahi University of Engineering and Technology, Rajshahi, Bangladesh.**Received:** May, 18, 2021**Revised:** August, 14, 2021**Accepted:** September, 02, 2021**Keywords**

Energy storage;
Bismuth titanate;
Refinement of XRD;
La and Nd co-doping;
Lattice distortion.

Abstract: Capacitive energy storage technology becomes more popular due to the fast charging facilities. Bismuth titanate (BIT) is a lead-free ferroelectric material used as a dielectric medium in the capacitive energy storage system. La and Nd co-doped BIT has been synthesized through a solid-state reaction process to obtain improved dielectric properties. Various characterization technologies such as Fourier Transform Infrared (FTIR) and X ray diffraction (XRD) have been done to sure the reaction completion and absence of the impurity phase of BIT. Rietveld refinement of XRD has been carried out to investigate the crystal structural properties of La and Nd-doped BIT. Capacitive energy storage performances have been tested by measuring the parallel plate capacitance and quality factor of BIT ceramics. Co-doped BIT possesses the highest crystal density, which results in a high Q factor. The unit cell of the TiO_6 octahedral of BIT becomes highly distorted as a consequence of La and Nd co-doping, which increases surface polarization, and the capacitance of BIT increases.

© 2021 The authors. Published by EDU Journal of Computer and Electrical Engineering. This is an open access article under the CC BY NC license.

1. INTRODUCTION

Ferroelectric ceramics are promising materials in the electro-ceramic field due to their diverse applications such as non-volatile memory, supercapacitor, electro-mechanical or optoelectrical transducer, etc. [1]. Lead-based ferroelectric materials are usually commercially used due to their higher performance and low cost [2]. Conversely, lead-based ferroelectric materials have some drawbacks, e.g., environmental hazards due to high lead content, fatigue failure, aging, etc. [3-6]. Therefore, extensive researches are going on to obtain a substitute for lead-based ferroelectric materials. Bismuth layered structured ferroelectric (BLSF) materials are reported as a promising group of materials, which consist of bismuth oxide layers $(\text{Bi}_2\text{O}_3)^{2+}$ and perovskite-like layers $(\text{A}_{n-1}\text{B}_n\text{O}_{3n+1})^{2-}$ along c-axis [7]. Among the BLSF family, Bismuth titanate, $\text{Bi}_4\text{Ti}_3\text{O}_{12}$ (BIT), has been considered an alternative of lead-based ferroelectric ceramics because of their enhanced performance, such as high dielectric constant, with high remnant polarization with high Curie temperature [4, 8]. Bismuth titanate ceramics are considered as the most promising candidate for piezoelectric [9], piezo-tribo nano generator [10], X-ray shielding [11], high-temperature sensor applications [12], and photocatalysis etc. [13]. Ferroelectric

capacitors have rising applications in pulse power applications as energy storage devices due to their extremely short discharge time (microsecond level), such as medical fibrillator, hybrid electric vehicle, etc. [14-17]. The application of BIT ceramics in ferroelectric capacitive energy storage is noteworthy due to their excellent energy storage performance with high thermal stability and fatigue endurance [18, 19]. However, BIT suffers from the high coercive force, high dielectric loss, and not enough high remnant polarization [20]. Several types of research have been carried out to improve the performance of BIT by doping or co-doping with suitable rare earth elements such as La, Nd, Mn, etc., in both Bi-site and Ti-site [21-24]. Islam, et al. [23] reported that La and Nd doping and co-doping in BIT possess higher performance in the high dielectric constant and low dielectric loss. The authors mentioned that the remnant polarization and dielectric constant increase due to the rise of structural distortion and lack of center of symmetry of the bismuth titanate octahedral. The objective of the research is to investigate the relationship between the structural distortion and performance of La and Nd doping in the BIT ferroelectric ceramics in capacitive energy storage applications. The research's output knowledge will help future site engineering in ferroelectric materials to obtain improved performance.

✉Corresponding author. E-mail address: aminulmse@gmail.com (Md. Aminul Islam)

This work is licensed under a Creative Commons Attribution 4.0. License (CC BY NC 4.0)

Available online at <http://edu-journals.com/index.php/ejcee><https://doi.org/10.46603/ejcee.v2i1.24>

2. EXPERIMENTAL PROCEDURE

2.1 Materials preparation method

Bismuth titanate (BIT) $\text{Bi}_4\text{Ti}_3\text{O}_{12}$, Neodymium (Nd) doped BIT $\text{Bi}_{3.15}\text{Nd}_{0.85}\text{Ti}_3\text{O}_{12}$ (BNT), Lanthanum (La) doped BIT $\text{Bi}_{3.25}\text{La}_{0.75}\text{Ti}_3\text{O}_{12}$ (BLT) and La & Nd co-doped BIT, $\text{Bi}_3(\text{La}_{0.5}\text{Nd}_{0.5})\text{Ti}_3\text{O}_{12}$ (BLNT) were prepared through conventional solid-state reaction method. Different types of commercially available starting powder materials such as bismuth oxide (Bi_2O_3) (99.9% pure, MERCK, Germany), lanthanum oxide (La_2O_3 , 99.9% pure, Wako pure chemical industries Ltd. Japan), Neodymium oxide (Nd_2O_3 , 99.9% pure, Wako pure chemical industries Ltd. Japan) have been used for the preparation of the material. The powders were taken according to the stoichiometric ratio of respective compositions of BIT, BNT, BLT and BLNT materials. The composition mentioned above of BNT, BLT and BLNT ceramics were chosen because of their best performance reported in the literature [23, 25-28]. An electronic weight balance has been used to weigh the powders. The powders were mixed together inside the ethanol by the ball milling process for 24 hours. 10% of excess Bi_2O_3 has been added to compensate for the evaporation of bismuth oxide during the calcining and sintering process [29]. After ball milling, the solution was settled down for 24 hours, and ethanol was separated out. The samples were further dried at 90°C for 2 hours to evaporate ethanol. The well-mixed powders were appropriately grounded in a mortar and pestle. The fine grounded powders were calcined at 800°C for two hours in a furnace under open-air conditions [30]. The calcite powders were characterized through Fourier Transform Infrared (FTIR) and X-ray diffraction (XRD) processes to ensure the final product materials formation. For dielectric properties measurement, the calcined powders were formed in the pellet of equal sizes. The exact amount of powders weighted and mixed with 2.5% polyvinyl alcohol (PVA) solution as binder and ground properly during pellet formation. The dry powders were pressed in a uniaxial direction at 60kN pressure by a hand pressure gauge, and pellets having a thickness of 0.15 cm and a radius of 0.65 cm are formed. The pellets were sintered at 950 °C temperature for 1 hour [30].

2.2 Characterization

The vibrational properties of the prepared samples have been investigated by using FTIR spectrophotometer (spectrum 100, Perkin Elmer). All infrared spectra of the samples were collected within the ranges of 2000 – 400 cm^{-1} with the instrument resolution of 1 cm^{-1} . For FTIR, the ceramic powders were finely grounded with desiccated highly purified (99.99%) alkali halide, KBr powder in a clean quartz mortar. The mixtures were then pressed by using a pressure gauge with a pressure of 60 kN to yield pellets of approximate thickness 0.11 mm, which is suitable for mounting into the spectrometer. X-ray diffraction of the prepared samples was performed using an X-ray diffractometer (D8 Advance, Bruker, Germany) to study the prepared sample's phase purity and crystal structure. X-ray diffraction pattern provides information about the sample homogeneity, phase, and orientation of the different crystallographic planes. Cu K_α radiation ($\lambda = 1.5405 \text{ \AA}$) was used for the excitation of atoms. The scanning drive axis is taken as two-theta and then scan in between 20 to 60° of 2 values for the samples of pure BIT, BLT, BNT, and BLNT. The values of Miller indices (hkl) were identified by adopting JCPDS card (reference code, 00-

035-0795) of bismuth titanate. The structural refinement of BIT and BLT, BNT BLNT has been carried out by the Rietveld method based on orthorhombic crystal structure with a non-conventional *B2cb* symmetry. Bruker's built-in software (EVA, TOPAS) has been used for the Rietveld refinement analysis [31, 32]. The quantitative analyses of the XED pattern were done by the TOPAS (Total pattern Analysis solution) software. The software is integrated with profile fitting techniques and other related applications such as Ab-initio structure determination, single line fittings and indexing [33]. The Thompson-Cox-hasting-pseudo-Voigt profile function was used to adjust diffractograms. Lorentzian fraction of the profile changes with the Gauss and Lorentz components of the full width of half maxima. The lattice parameters, atomic position, occupation factors, linear absorption coefficient, crystal density, and size were calculated by using the Rietveld procedure [34]. Since the La and Nd substitution leads to a marked change in the in-plane crystal structure in BIT, compared with the monoclinic distortion, the structural change induced by the La substitution can be explained by the orthorhombic *B2cb* [35]. The dielectric properties such as impedance and Q factor of the bulk ceramic samples were measured using Precision Impedance Analyzer (Wayne Kerr Electronics 6500B series). Before dielectric measurement, both side surfaces of samples were coated with silver paste. The dielectric properties have been scanned with a frequency range from 100 Hz to 1 MHz at AC signal of 300mV.

3. RESULTS AND DISCUSSIONS

3.1 FTIR spectroscopy

Figure 1. FTIR spectra of BIT, BLT, BNT, BLNT ceramic powders shows the FTIR spectrum of the BIT, BNT, BLT and BLNT ceramic powders calcined at a temperature of 800 °C for 2 hours. All of the FTIR spectrums were recorded at room temperature. There are various peaks at 1630 cm^{-1} , 1384 cm^{-1} , 937 cm^{-1} , 812 cm^{-1} , 594 cm^{-1} and 404 cm^{-1} have been observed for BIT ceramic. The sharp bands at 812 cm^{-1} and 594 cm^{-1} correspond to the stretching vibrations of Ti–O bonds [36], while the peak at 404 cm^{-1} corresponds to the bending vibrations of Ti–O bonds in the TiO_6 octahedron [37]. The appearance of these absorptions is a characteristic feature of the formation of titanate octahedral. The former two bands, i.e., 1630 and 1384 cm^{-1} correspond to the bending vibrations Bi-O bond and 937 cm^{-1} correspond to the stretching vibration of Bi-O bond [3]. It is also found that the IR spectra of BLT, BNT, and BLNT powders are similar features to that of BIT powder, except small shifting of the absorption peaks. As a consequence of La and Nd doping, the peaks that correspond to Ti–O bonds in the TiO_6 octahedron have been found to be shifted from the pure BIT's peaks and the peaks that correspond to the Bi-O bond are quite unchanged. The absorption peaks at 812 and 594 cm^{-1} are shifted to higher wavenumbers of 817 cm^{-1} and 602 cm^{-1} in the IR spectra of BLT and BNT due to the substitution of Bi by La and Nd respectively. On the other hand, the absorption peaks at 812 and 594 cm^{-1} are shifted to higher wavenumbers of 817 cm^{-1} and 633 cm^{-1} in the IR spectra of BLNT. These results conclude that the addition of La and Nd creates some modification in the lattice constant of TiO_6 octahedron of bismuth titanate.

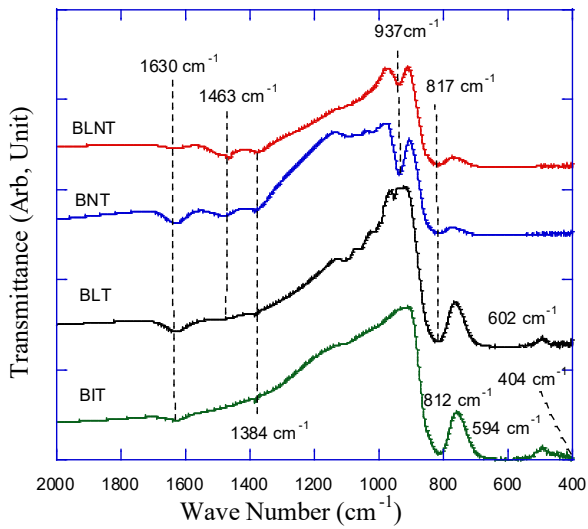


Figure 1. FTIR spectra of BIT, BLT, BNT, BLNT ceramic powders

3.2 XRD

The structural properties have been investigated by XRD. Figure 2 shows the XRD of BIT and BNT and BLT and BLNT. All the

XRD pattern matches with the JCPDS reference code, 01-076-7805, so no impurity phase has been found. From the Rietveld refinement results, different parameters such as lattice constants, unit cell volume, and crystal density have been determined. The R_{Bragg} values were in-between range 6.65-9.09 as shown in Table 1. The highest unit cell volume was obtained for BLT, followed by BIT and BNT, and BLNT holds the lowest unit cell volume. On the other hand, BLNT possesses the highest crystal density and is then followed by BNT and BIT. The BLT ceramic holds the lowest crystal density. Due to La and Nd individual doping, the crystal density of BIT does not alter significantly. But due to co-doping, the density increases drastically, which predicts the reduction porosity within the crystals. Almost similar crystal sizes have been found for the different ceramics. Lattice parameters of BIT are distorted as a consequence of doping with atoms having different diameters. The tetragonal distortion (c/a) of BLT, BNT and BLNT ceramics are 6.035334, 6.038299, and 6.045937 respectively. The highest distortion belongs to co-doped BLNT ceramic.

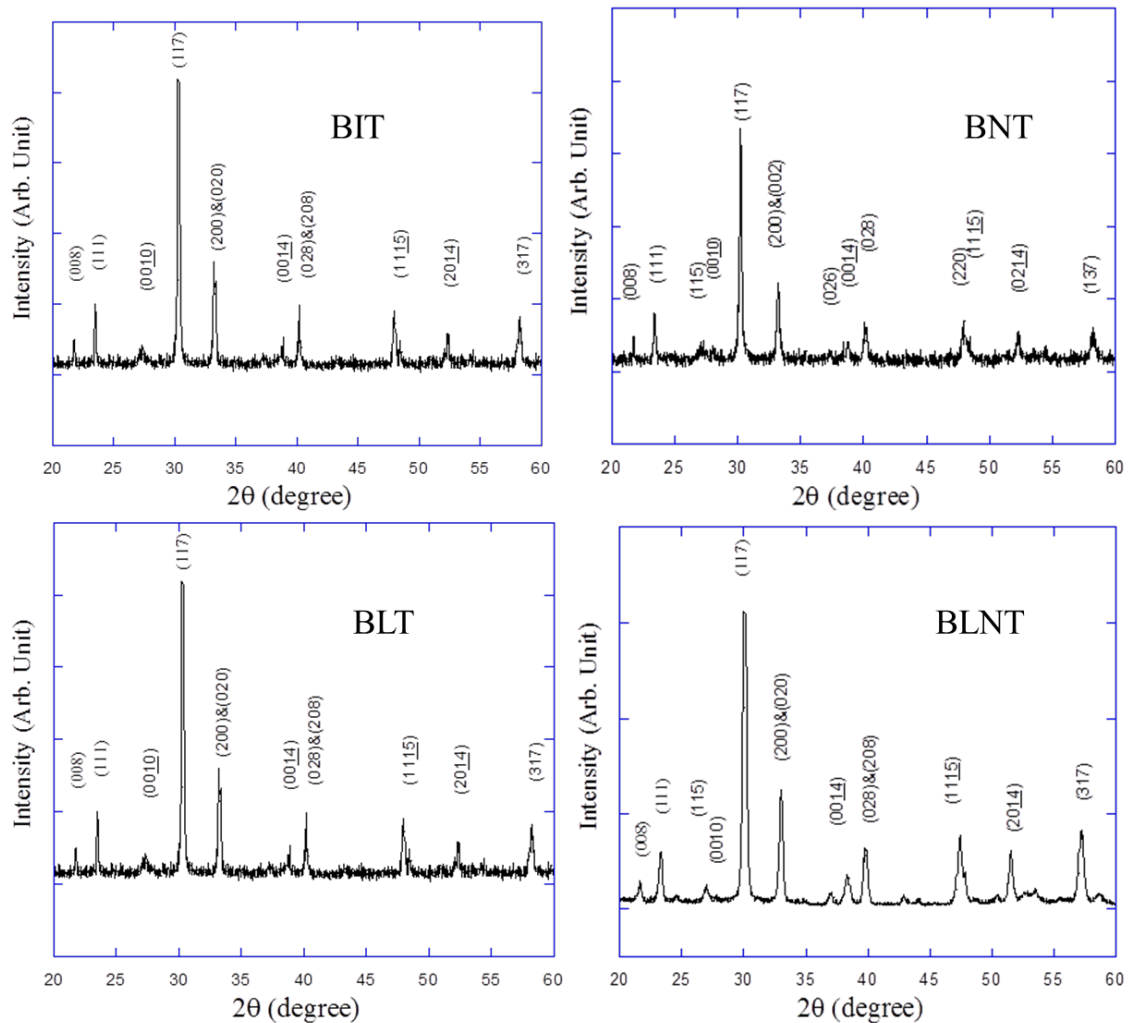


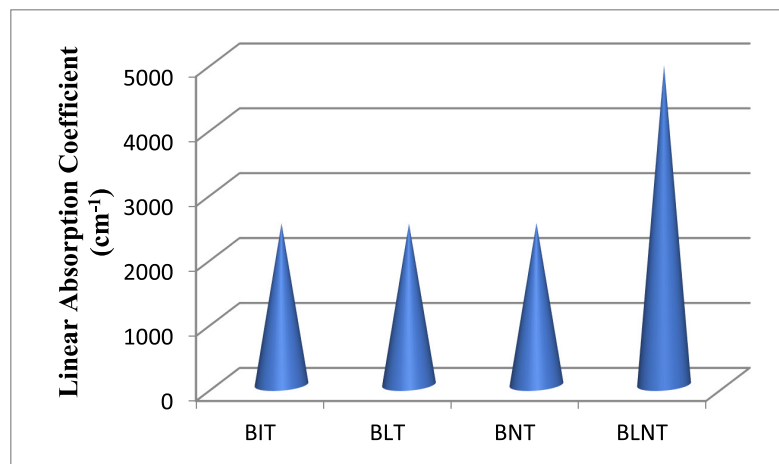
Figure 2. The X-ray diffraction patterns of BIT, BLT, BNT and BLNT powders calcined at 800°C temperature for 2 hours

Table 1. Lattice parameters, cell volume and crystal density of calcined powders retrieved from the refinement of XRD

Name	R_{Bragg}	Lattice parameters (Å)			Unit Cell Volume (Å ³)	Crystal density (g/cm ³)	Crystal size Lorentzian (nm)
		a	b	c			
BIT	9.09	5.4317(14)	5.4142(13)	32.7749(79)	963.85(42)	8.0734(35)	68.2(23)
BLT	7.07	5.4338(16)	5.4192(16)	32.7948(86)	965.70(47)	8.0580(39)	69.7(54)
BNT	7.13	5.42787(99)	5.40776(98)	32.7751(45)	962.03(28)	8.0887(23)	48.8(30)
BLNT	6.65	5.4205(27)	5.4085(23)	32.772(14)	960.79(75)	25.291(20)	64.1(21)

Figure 3 represents the linear absorption coefficient (LAC) of X-ray values of BIT, BNT, BLT and BLNT ceramics. Linear absorption coefficient describes the fraction of the beam of X-ray that is absorbed per thickness of materials. The highest LAC value has been found for co-doped BLNT ceramic. A higher LAC value means higher interaction of photons with the particles of the

material. This can be due to the increased density characteristic of BLNT ceramic. Table 2 shows the atomic position in X, Y and Z direction within unit cell. Due to co-doping, BLNT ceramic unit cell distorted and atomic positions are changed from their original site.

**Figure 3.** Linear absorption coefficient of different calcined powders**Table 3.** Atomic site positions of BIT and BLNT ceramics**Table 2** Lattice parameters, cell volume and crystal density of calcined powders retrieved from the refinement of XRD

Sample	Atom	Site	X	Y	Z
BIT	Bi	Bi1	0.00000	0.00000	0.06700
	Bi	Bi2	0.00000	0.00000	0.21100
	Ti	Ti1	0.00000	0.00000	0.50000
	Ti	Ti2	0.00000	0.00000	0.37200
	O	O1	0.25000	0.25000	0.00000
	O	O2	0.25000	0.25000	0.25000
	O	O3	0.00000	0.00000	0.43600
	O	O4	0.00000	0.00000	0.30800
BLNT	O	O5	0.25000	0.25000	0.12800
	Bi	Bi1	0.0(18)	0.0(18)	0.07077(17)
	Bi	Bi2	0.0(18)	0.0(18)	0.20808(14)
	Ti	Ti1	0.0(18)	0.0(18)	0.47996(49)
	Ti	Ti2	0.0(18)	0.0(18)	0.3636(50)
	O	O1	0.115(36)	0.118(36)	-0.0173(15)
	O	O2	0.188(57)	0.302(55)	0.2291(15)
	O	O3	0.0(18)	0.0(18)	0.4212(15)
O	O4	0.0(18)	0.0(18)	0.363(16)	
O	O5	0.2(80)	0.3(76)	0.1187(15)	

3.3 Energy storage capability in terms of Capacitance

The energy storage capability of ceramic has been examined by measuring the capacitance. Figure 4 shows the capacitances at different frequencies for the BNT, BLT and BLNT ceramics. All samples possess higher capacitance values at low-frequency range and capacitance decreases with the increase of frequency and becomes approximately more or less constant above 10kHz frequency range. The capacitance value of ceramic materials depends on their polarizability. These four kinds of polarization mechanisms such as electronic, dipolar or rotational, ionic and space charges. The effectiveness of each mechanism lies in a characteristic range. At low-frequency range, all mechanisms of polarization are active; that is why the capacitance of all samples

was high. At higher frequency range above 10kHz space charge, ionic and orientational mechanisms of polarization are ceased, and only electronic mechanism contributes. So that at higher frequencies, capacitance decreases. The obtained capacitance values (at 100 Hz frequency and room temperature) were 323, 101 and 78 pF for BLNT, BLT and BNT ceramic respectively. At high frequency (1MHz) and room temperature, the capacitance values of BLNT, BLT and BNT ceramic were 73, 52 and 41 pF, respectively. Long et al. [38] also reported similar capacitive properties of Bismuth titanate (BIT) $\text{Bi}_4\text{Ti}_3\text{O}_{12}$ with a capacitance value of 5nF/cm at 1 Hz and 250 °C temperature. Simoes et al. [39] reported 1 nF capacitance value for BLT thin film at 100 KHz and room temperature.

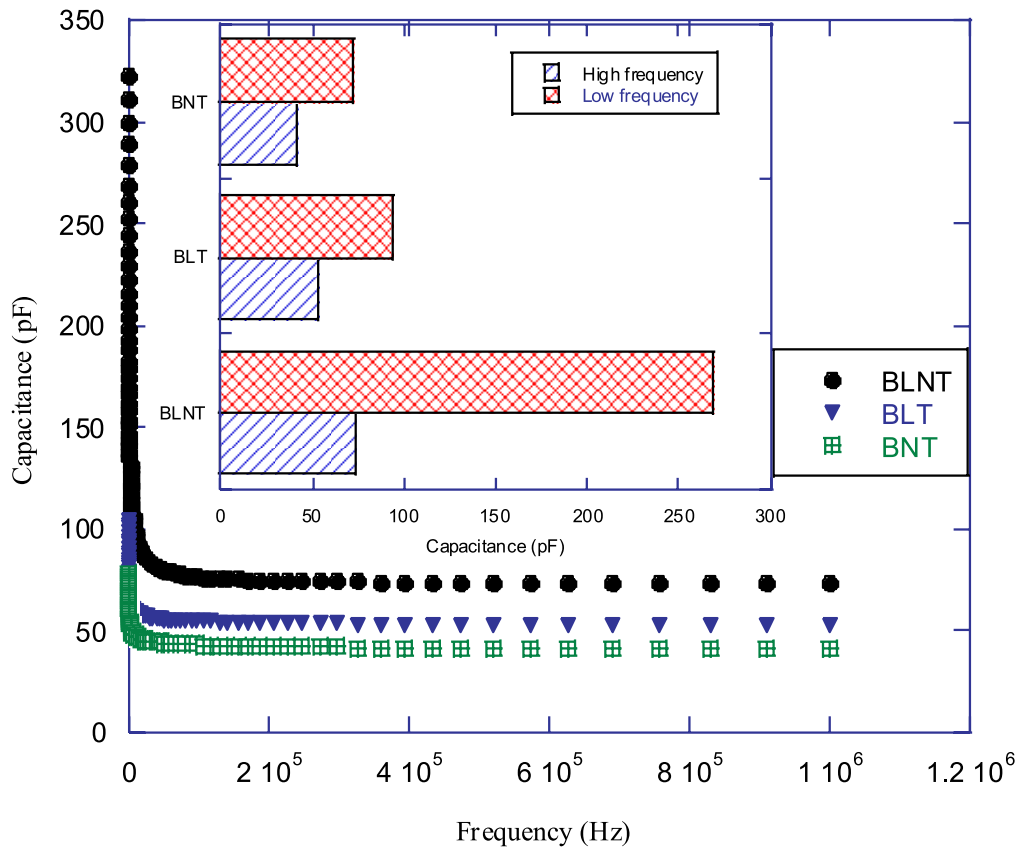


Figure 4. Frequency-dependent capacitance of BLNT, BNT, and BLT ceramics; Capacitance values at low frequency (100 Hz) and High frequency (100kHz)

3.3 Quality Factor or Q factor

Quality factor or Q factor of a capacitor is the efficiency of that capacitor in terms of energy losses. In the case of the AC signal, the Q factor of a capacitor represents the ratio of energy stored to the dissipated energy as thermal losses. The capacitor quality factor 'Q' has been extracted by the following relation [40].

$$Q = \frac{\text{imaginary}(Z)}{\text{real}(Z)} \tag{1}$$

Where Z is impedance. Figure 5. Frequency-dependent Q factor characteristic of BLNT, BNT, BLT and BIT ceramics shows the frequency-dependent Q factor of BLNT, BLT, BNT and BIT ceramics. The Q factor value increases slightly due to both La and Nd singular doping. But in the case of co-doping, the Q factor value increases drastically. This is due to the

suppression of vacancies created as a result of the evaporation of bismuth oxides during the processing. A considerable amount of oxygen vacancies are introduced and eventually, free electrons are generated according to the following equation.

$$\text{O}_o = \text{V}_o^{**} + 2e + 1/2\text{O}_2 \tag{2}$$

Where O_o is the oxygen ion at parent crystal site, V_o^{**} is the intrinsic oxygen vacancy and e is the free electron. From this equation, it is obvious that free electrons increase with the increase of sintering temperature and eventually enhances the leakage current. It is well known that La and Nd are less volatile than the Bi atom. Therefore, substitutions of volatile Bismuth atom by comparatively less volatile La & Nd, effectively suppress the intrinsic oxygen vacancies. The highest suppression might be happened due to co-doping for composition at $[\text{Bi}_3(\text{La}_x\text{Nd}_{1-x})\text{Ti}_3\text{O}_{12}]$ where X=0.5].

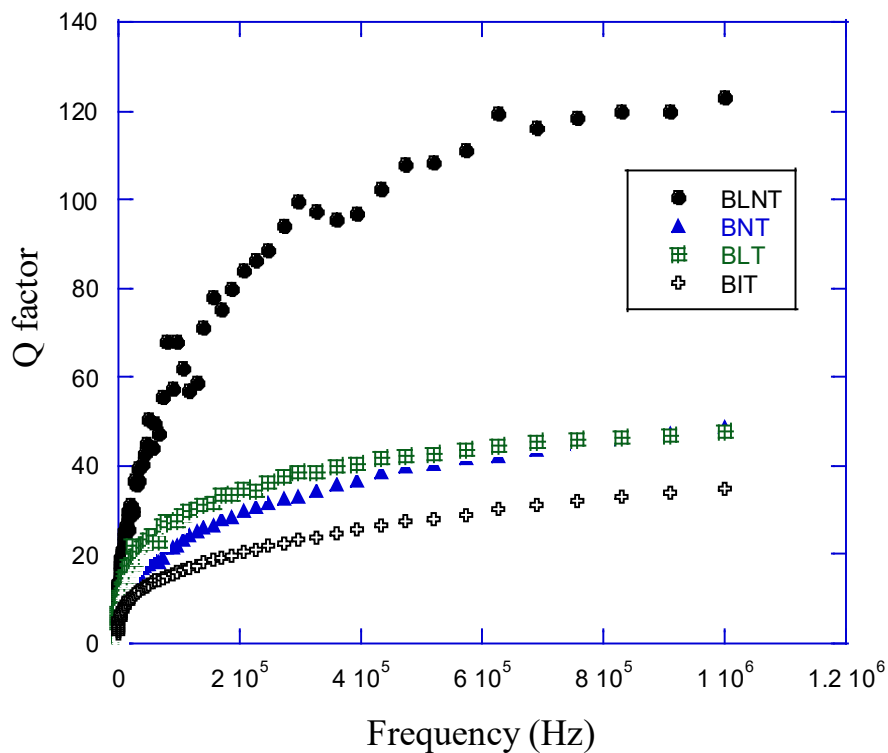


Figure 5. Frequency-dependent Q factor characteristic of BLNT, BNT, BLT and BIT ceramics

4. CONCLUSION

Bismuth Titanate (BIT) doped with La and Nd ceramics have been synthesis through solid-state reaction method. FTIR spectrum predicts reaction completion for the BIT formation. From the XRD, it has been confirmed that there was no impurities phase in both pure BIT and La and Nd-doped BIT. The Rietveld refinement of XRD reveals the structural properties of doped and undoped BIT. A drastic increase of crystal density and linear absorption of coefficient BIT have been found due to La and Nd co-doping. As a consequence of La and Nd co-doping, and augmented lattice distortion of the TiO_6 octahedral unit cell of BIT has been found, which results in an increase in polarization as well as the capacitance of BIT ceramics. The highest quality factor value has been observed for La and Nd co-doped BIT.

REFERENCES

- [1] S. M. Said, M. F. M. Sabri, and F. Salleh, "Ferroelectrics and Their Applications," in *Reference Module in Materials Science and Materials Engineering*: Elsevier, 2017.
- [2] J. Rödel, K. G. Webber, R. Dittmer, W. Jo, M. Kimura, and D. Damjanovic, "Transferring lead-free piezoelectric ceramics into application," *Journal of the European Ceramic Society*, vol. 35, no. 6, pp. 1659-1681, 2015/06/01/ 2015.
- [3] O. Subohi, G. S. Kumar, M. M. Malik, and R. Kurchania, "Dielectric properties of Bismuth Titanate ($\text{Bi}_4\text{Ti}_3\text{O}_{12}$) synthesized using solution combustion route," *Physica B: Condensed Matter*, vol. 407, no. 18, pp. 3813-3817, 2012/09/15/ 2012.
- [4] M. Muneeswaran, B. C. Choi, S. H. Chang, and J. H. Jung, "Effect of dysprosium doping on structural and vibrational properties of lead-free ($\text{Na}_{0.7}\text{K}_{0.3}$) $0.5\text{Bi}_{0.5}\text{TiO}_3$ ferroelectric ceramics," *Ceramics International*, vol. 43, no. 16, pp. 13696-13701, 2017/11/01/ 2017.
- [5] X. Lv, J. Zhu, D. Xiao, X.-x. Zhang, and J. Wu, "Emerging new phase boundary in potassium sodium-niobate based ceramics," *Chemical Society Reviews*, 10.1039/C9CS00432G vol. 49, no. 3, pp. 671-707, 2020.
- [6] H. Tao *et al.*, "Ultrahigh Performance in Lead-Free Piezoceramics Utilizing a Relaxor Slush Polar State with Multiphase Coexistence," *Journal of the American Chemical Society*, vol. 141, no. 35, pp. 13987-13994, 2019/09/04 2019.
- [7] S. Ma, X. Cheng, Z. Ma, Z. Xu, and R. Chu, "Characterization of highly (117)-oriented $\text{Bi}_3.2\text{SLa}_{0.75}\text{Ti}_3\text{O}_{12}$ thin films prepared by rf-magnetron sputtering technique," *Solid State Communications*, vol. 278, pp. 31-35, 2018/09/01/ 2018.
- [8] P. Y. Fan *et al.*, "Large strain with low hysteresis in $\text{Bi}_4\text{Ti}_3\text{O}_{12}$ modified $\text{Bi}_{1/2}(\text{Na}_{0.82}\text{K}_{0.18})(1/2)\text{TiO}_3$ lead-free piezoceramics," *Journal of the European Ceramic Society*, vol. 38, no. 13, pp. 4404-4413, Oct 2018.
- [9] Q. Xu *et al.*, "Bismuth titanate based piezoceramics: Structural evolutions and electrical behaviors at different sintering temperatures," *Journal of Alloys and Compounds*, vol. 882, p. 160637, 2021/11/15/ 2021.
- [10] S. Hajra, A. M. Padhan, M. Sahu, P. Alagarsamy, K. Lee, and H. J. Kim, "Lead-free flexible Bismuth Titanate-PDMS composites: A multifunctional colossal dielectric material for hybrid piezo-triboelectric nanogenerator to sustainably power portable electronics," *Nano Energy*, vol. 89, p. 106316, 2021/11/01/ 2021.
- [11] L. Yu, P. L. Yap, A. Santos, D. Tran, and D. Losic, "Lightweight Bismuth Titanate ($\text{Bi}_4\text{Ti}_3\text{O}_{12}$) Nanoparticle-Epoxy Composite for Advanced Lead-Free X-ray Radiation Shielding," *ACS Applied Nano Materials*, vol. 4,

no. 7, pp. 7471-7478, 2021/07/23 2021.

- [12] P. Sivagnanapalani, N. I. Ansari, and P. K. Panda, "Calcium Bismuth Titanate with High Curie Temperature (T_c) for High-Temperature Sensor Applications," *Journal of Electronic Materials*, vol. 50, no. 8, pp. 4806-4811, 2021/08/01 2021.
- [13] S. Khodadoost, A. Hadi, J. Karimi-Sabet, M. Mehdipourghazi, and A. Golzary, "Optimization of hydrothermal synthesis of Bismuth titanate nanoparticles and application for photocatalytic degradation of Tetracycline," *Journal of environmental chemical engineering*, vol. 5, pp. 5369-5380, 2017.
- [14] R. Kang *et al.*, "Domain Engineered Lead-Free Ceramics with Large Energy Storage Density and Ultra-High Efficiency under Low Electric Fields," *ACS Applied Materials & Interfaces*, vol. 13, no. 21, pp. 25143-25152, 2021/06/02 2021.
- [15] D. Song *et al.*, "Energy storage in BaBi 4 Ti 4 O 15 thin films with high efficiency," *Journal of Applied Physics*, vol. 125, no. 13, p. 134101, 2019.
- [16] S. Bian, Z. Yue, Y. Shi, J. Zhang, and W. Feng, "Ultrahigh energy storage density and charge-discharge performance in novel sodium bismuth titanate-based ceramics," *Journal of American Chemical Society*, vol. 104, no. 2, pp. 936-947, 2021.
- [17] Y. Xie *et al.*, "Large energy-storage density with good dielectric property in bismuth sodium titanate-based thin films," *Journal of Alloys and Compounds*, vol. 884, p. 161031, 2021/12/05/ 2021.
- [18] D. P. Song *et al.*, "Energy storage in BaBi 4 Ti 4 O 15 thin films with high efficiency," vol. 125, no. 13, p. 134101, 2019.
- [19] W. P. Cao *et al.*, "High-Energy Storage Density and Efficiency of (1-x) 0.94 NBT-0.06 BT -xST Lead-Free Ceramics," (in English), *Energy Technology*, Article vol. 3, no. 12, pp. 1198-1204, Dec 2015.
- [20] Z. Xiao *et al.*, "Bismuth lanthanum titanate ceramics from amorphous precursors activated by using mechanochemical treatment," *Ceramics International*, vol. 44, no. 11, pp. 13106-13112, 2018/08/01/ 2018.
- [21] E. V. Ramana *et al.*, "Effect of samarium and vanadium co-doping on structure, ferroelectric and photocatalytic properties of bismuth titanate," *RSC Advances*, 10.1039/C7RA00021A vol. 7, no. 16, pp. 9680-9692, 2017.
- [22] Y. Idemoto, S. Akabane, N. Ishida, and N. Kitamura, "Ferroelectric properties, average and local structures of (Bi, RE)(4)(Ti, Nb)(3)O-12 (RE = La, Pr, Nd)," *Japanese Journal of Applied Physics*, vol. 56, no. 10, Oct 2017, Art. no. 101501.
- [23] M. A. Islam, M. S. Islam, and M. A. Gafur, "Synthesis and Characterization of La and Nd Co-Doped Bismuth Titanate Ferroelectric Ceramics," *International Journal of Applied Ceramic Technology*, vol. 12, pp. E191-E196, 2015.
- [24] M. A. Islam, M. M. Rahman, M. S. Parvez, M. S. Islam, M. Hasanuzzaman, and W. P. Hew, "Tangible effect of Mn on the dielectric properties of Nd doped Bismuth Titanate ceramic," *Journal of The Australian Ceramic Society*, vol. 52, no. 1, pp. 89-94, 2016.
- [25] P. Siriprapa, A. Watcharapasorn, and S. Jiansirisomboon, "Effects of Mn-dopant on phase, microstructure and electrical properties in Bi3.25La0.75Ti3O12 ceramics," (in English), *Ceramics International*, Article; Proceedings Paper vol. 39, pp. S355-S358, 2013.
- [26] J. Y. Han and C. W. Bark, "Influence of transition metal doping (X = Co, Fe) on structural, optical properties of Ferroelectric Bi3.25La0.75X1Ti2O12," (in English), *Nano Convergence*, Article vol. 2, p. 5, 2015, Art. no. 7.
- [27] A. Garg, Z. H. Barber, M. Dawber, J. F. Scott, A. Snedden, and P. Lightfoot, "Orientation dependence of ferroelectric properties of pulsed-laser-ablated Bi4-xNdxTi3O12 films," (in English), *Applied Physics Letters*, Article vol. 83, no. 12, pp. 2414-2416, Sep 2003.
- [28] E. Y. Kim *et al.*, "Effects of deposition temperatures of Nd-doped Bi4Ti3O12 thin films prepared by pulsed laser deposition," (in English), *Ferroelectrics*, Article; Proceedings Paper vol. 533, no. 1, pp. 56-62, 2018.
- [29] M. A. Islam, A. Gafur, and M. S. Islam, "Effects of Excess Bi2O3 on the Properties of La- doped Bismuth titanate (Bi4Ti3O12) Ferroelectric Ceramics," *Asian Journal of Applied Sciences & Engineering ;*, vol. 1, no. 2, pp. 65-69, 2012.
- [30] A. M. Islam, M. Gafur, and S. M. Islam, "Sintering characteristics of La/Nd doped Bi4Ti3O12 bismuth titanate ceramics," *Science of Sintering*, vol. 47, no. 2, pp. 175-186, 2015.
- [31] W. L. Bevilacqua *et al.*, "Revealing the Dynamic Transformation of Austenite to Bainite during Uniaxial Warm Compression through In-Situ Synchrotron X-ray Diffraction," *Metals*, vol. 11, no. 3, p. 467, 2021.
- [32] R. A. Chowdhury, S. A. Dhar, S. Das, M. K. Nahian, and M. Rakibul Qadir, "Green synthesis and characterization of silver nanoparticles from the aqueous extract of the leaves of Citrus aurantifolia," *Materials Today: Proceedings*, vol. 44, pp. 1039-1042, 2021/01/01/ 2021.
- [33] M. Tamer, "Quantitative Phase Analysis Based on Rietveld Structure Refinement for Carbonate Rocks," *Journal of Modern Physics*, vol. 4, pp. 1149-1157, 2013.
- [34] A. Scaltsoyiannes, A. Antzaras, G. Koilaridis, and A. Lemonidou, "Towards a generalized carbonation kinetic model for CaO-based materials using a modified random pore model," *Chemical Engineering Journal*, vol. 407, p. 127207, 2021/03/01/ 2021.
- [35] S. J. Kim *et al.*, "Direct observation of oxygen stabilization in layered ferroelectric Bi3.25La0.75Ti3O12," *Applied Physics Letters*, vol. 91, no. 6, p. 062913, 2007/08/06 2007.
- [36] N. Ren *et al.*, "In situ construction of a titanate-silver nanoparticle-titanate sandwich nanostructure on a metallic titanium surface for bacteriostatic and biocompatible implants," *Journal of Materials Chemistry*, 10.1039/C2JM32434B vol. 22, no. 36, pp. 19151-19160, 2012.
- [37] W. Hu, L. Li, G. Li, Y. Liu, and R. L. Withers, "Atomic-scale control of TiO6 octahedra through solution chemistry towards giant dielectric response," *Scientific Reports*, Article vol. 4, p. 6582, 10/10/online 2014.
- [38] C. Long, Q. Chang, and H. Fan, "Differences in nature of electrical conductions among Bi4Ti3O12-based ferroelectric polycrystalline ceramics," *Scientific Reports*, vol. 7, no. 1, p. 4193, 2017/06/23 2017.
- [39] A. Simoes *et al.*, "Ferroelectric and dielectric properties of lanthanum-modified bismuth titanate thin films obtained by the polymeric precursor method," vol. 13, no. 1-3, pp. 65-70, 2004.
- [40] A. Tombak *et al.*, "Tunable barium strontium titanate thin film capacitors for RF and microwave applications," *IEEE Microwave and Wireless Components Letters*, vol. 12, no. 1, pp. 3-5, 2002.